International Journal of Pharmaceutics: X 7 (2024) 100230

Contents lists available at ScienceDirect

International Journal of Pharmaceutics: X

journal homepage: www.sciencedirect.com/journal/international-journal-of-pharmaceutics-x

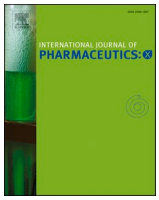

Everolimus-encapsulation in Pluronic P123 self-assembled micelles as drug delivery systems for drug-coated balloons

Mohammad Akrami-Hasan-Kohal [a], Adrien Chouchou [b], Sébastien Blanquer [a], Tahmer Sharkawi [a,*]

[a] ICGM, Univ Montpellier, CNRS, ENSCM, Montpellier, France
[b] IBMM, Université de Montpellier, CNRS, ENSCM, 34000 Montpellier, France

ARTICLE INFO

Keywords:
Drug-coated balloons
Everolimus
Pluronic P123
Micelles
Excipient
Drug delivery

ABSTRACT

Drug-coated balloons (DCBs) are effective tools for cardiovascular interventions, ensuring uniform drug delivery to occluded arteries. This research investigates the potential of Pluronic P123 (P123), a micelle-forming polymer, to solubilize and release Everolimus (EVE) from DCBs. Furthermore, it seeks to understand how the ratio of P123 to EVE affects release rates and micelle formation under physiological conditions. We tested three P123 to EVE ratios: 90:10, 75:25, and 50:50. Microscopy revealed that increasing EVE proportions resulted in more uniform coatings. Fourier-transform infrared spectroscopy (FTIR) analysis confirmed the successful incorporation of EVE into the P123 matrix without altering its chemical properties. Differential scanning calorimetry (DSC) studies showed that EVE incorporation affected the crystalline structure of P123, leading to more uniform coatings. In vitro release studies showed that all formulations had <1% drug loss in the first minute (the tracking phase); furthermore, the 90:10 ratio exhibited optimal drug release in the following 3 min, corresponding to the deployment phase in DCB angioplasty. Analysis of micelle loading capacity (LC), encapsulation efficiency (EE), size, and structure indicated an increase in both LC and EE with higher EVE content and a corresponding enlargement in micelle size. Given these findings, the optimized formula provided a consistent coating on commercial balloons, highlighting the potential of using P123 for DCB drug coating and release.

1. Introduction

Atherosclerosis, a significant predisposing factor for cardiovascular disease (CVD), remains the predominant cause of mortality worldwide (Jebari-Benslaiman et al., 2022), (Libby et al., 2019). This disease involves endothelium activation, a phenomenon that precipitates a sequence of events including lipid accumulation, fibrous element deposition, and calcification. These processes lead to the narrowing of blood vessels and ignite inflammatory pathways (Jebari-Benslaiman et al., 2022). The resultant atheroma plaque formation engenders cardiovascular complications (Jebari-Benslaiman et al., 2022). Given the ubiquitous prevalence of CVDs and the mounting societal and economic implications, a compelling case can be made for the exploration and enhancement of current therapeutic strategies (Xue et al., 2023), (Wang et al., 2023b).

Reflecting on the critical need for advanced therapeutic strategies in combating CVDs, we turn our focus to innovative treatment options. One promising approach involves the use of drug-coated balloons (DCBs), recognized for their effectiveness in treating a range of cardiovascular diseases. DCBs function by opening up occluded arteries and delivering antiproliferative drugs locally to impede restenosis (Lee et al., 2020), (Giacoppo et al., 2023), (Dash et al., 2022), (Li et al., 2022), (Cai et al., 2022), (Yerasi et al., 2020). The DCB angioplasty technique allows for the delivery of antiproliferative drugs into the arterial wall during balloon inflation and leaves no residual structure (Kasbaoui et al., 2023). Moreover, DCBs proffer potential long-term benefits over stent-related adverse effects that can instigate restenosis, thrombosis, and accelerated neoatherosclerosis (Giacoppo et al., 2023), (Abbott et al., 2023), (Ali et al., 2019). Despite these advantages and because of certain drawbacks, the current recommendation limits the use of DCBs in certain scenarios. They are used mainly where stents are deemed unsuitable in the treatment of coronary artery disease and peripheral artery disease, such as in-stent restenosis, small vessel lesions, and bifurcation lesions (Wang et al., 2020), (Cortese et al., 2020), (Giacoppo

* Corresponding author.
E-mail address: tahmer.sharkawi@umontpellier.fr (T. Sharkawi).

https://doi.org/10.1016/j.ijpx.2024.100230
Received 22 October 2023; Received in revised form 20 December 2023; Accepted 8 January 2024
Available online 10 January 2024

et al., 2020).

However, while DCBs offer a significant advancement in the treatment of cardiovascular diseases, they are not without their challenges and limitations. This becomes evident when examining the intricacies of their current usage and effectiveness. Current DCBs use carriers like shellac resin, butyryl trihexyl citrate plasticizer, iopromide contrast medium, urea, and polysorbate emulsifier mainly to boost drug penetration into tissue, not for effective drug delivery at the disease site. A significant issue with these DCBs is uncontrolled drug release, leading to drug loss during tracking and inefficient therapeutic dose delivery (Anderson et al., 2016). Studies have shown that current DCBs lead to excessive drug loss rates (60–70%) and comparatively inferior drug transfer rates (< 20%) (Ang et al., 2018). Additionally, certain DCBs generate many particulates, posing safety risks like micro-occlusions and subsequent tissue damage. Higher-dose coatings can increase thrombotic occlusion risk, and embolization may contribute to high amputation rates seen in trials. These issues highlight the need for improved drug coating systems and strategies to limit particulate embolization (Ang et al., 2018).

In light of these challenges, recent advancements in computational modeling have significantly contributed to the understanding and enhancement of drug delivery mechanisms in DCBs. These models, varying in complexity from 1D to 3D, are instrumental in analyzing drug transport dynamics, including diffusion and advection, and the role of drug binding within the arterial wall. The unique challenges posed by the short drug delivery window of DCBs and the need for high drug loading have been addressed in these models (Escuer et al., 2022). For instance, Tzafriri et al.'s research (Tzafriri et al., 2019) presents an example where a coupled reaction-diffusion model was developed to understand the dissolution and tissue distribution of paclitaxel-coated balloons. This model predicts the kinetics of tissue-delivered drugs, focusing on the relative dissolution rates and the residual amounts of the coating, both in the lumen and tissue-embedded, as well as the concentration of the dissolved drug during and post-dissolution. These computational efforts align with our study's objective to optimize drug release from DCBs, ensuring effective and safe drug transfer to the arterial wall.

Building on the discussion of the limitations inherent in current DCB technologies, it is crucial to examine the specific characteristics of the antiproliferative drugs used for coating these balloons. Balloons can be coated with antiproliferative drugs like Taxanes, predominantly Paclitaxel, or Limus drugs such as Sirolimus, Tacrolimus, and Everolimus (EVE) (Wang et al., 2023a). In the realm of DCBs, Paclitaxel is commonly used for its antiproliferative effects, but concerns about its cytotoxicity have shifted focus to limus drugs like sirolimus and EVE. These alternatives offer similar benefits without inducing apoptosis and require smaller doses (Lee et al., 2023). EVE has demonstrated inhibitory action against kinase, specifically the mammalian target of rapamycin (mTOR), which is advantageous in averting atherosclerosis formation (Jumat et al., 2022). Additionally, this drug exhibits the capacity to suppress the proliferation of smooth muscle cells, thereby forestalling in-stent restenosis and neointimal hyperplasia (Jumat et al., 2022), (Akhmetzhan et al., 2023), (Park et al., 2018).

The aim of this study is to develop a coating for DCBs that reduces drug washout and maximizes drug delivery to lesion sites. Our focus is on designing a formulation with EVE-loaded Pluronic P123, intending to enhance the efficiency and effectiveness of DCBs in cardiovascular treatments. P123 has been extensively studied as an amphiphilic drug delivery polymer capable of encapsulating hydrophobic drugs within their micelle structure. It is known to be a non-toxic drug delivery vehicle with minimal adverse effects (Nguyen et al., 2021), (Batrakova and Kabanov, 2008), (Anirudhan et al., 2021), (Sastry and Hoffmann, 2004), (Kouser Qadri et al., 2022). P123 is a tri-block amphiphilic copolymer consisting of PEO20-PPO68-PEO20 with hydrophilic PEO segments and hydrophobic PPO segments allowing it to form micelles in water at low concentrations. This intrinsic characteristic allows the loading of large quantities of hydrophobic drugs within the hydrophobic core of PPO segments of P123 (Nguyen et al., 2021), (Batrakova and Kabanov, 2008). This versatile polymer can be used as a drug carrier in a diverse array of forms, including vesicles, micelles, mixed micelles, in-situ gels, tablets, and emulsions (Nguyen et al., 2021), (Sastry and Hoffmann, 2004). P123 forms micelles with a hydrophobic core that is ideally suited for encapsulating drugs with poor water solubility (Patel et al., 2022). Furthermore, amphiphilic excipients facilitate uniform dispersion of the hydrophobic drug during the coating process, likely aiding the tracking of DCBs with minimal drug loss (Xiong et al., 2016). With the unique properties of Pluronic outlined, and its suitability as a carrier for EVE established, we then delve into the crucial aspect of our research: the formulation. This includes examining various EVE to P123 ratios, an essential part of the process aimed at optimizing drug delivery in DCBs for enhanced treatment efficacy in cardiovascular diseases.

For this purpose, EVE-loaded P123 was prepared in varying ratios and applied onto a PEBAX angioplasty balloon substrate thin film, serving as a surrogate for drug-eluting balloon surfaces, using a micro-pipetting technique. The physical and chemical attributes of the prepared coatings were initially analyzed using scanning electron microscopy (SEM), Fourier-transformed infrared spectroscopy (FTIR), and differential scanning calorimetry (DSC). Furthermore, the release profile of EVE from the coatings was determined through High-Performance Liquid Chromatography-Ultraviolet Detection (HPLC-UV). Finally, the study characterized the micelle formations from the coatings using Transmission Electron Microscopy (TEM) and Dynamic Light Scattering (DLS). Feasibility was demonstrated for the optimal coating formulation by coating commercial angioplasty balloons.

2. Materials and methods

2.1. Materials

PEBAX® 7233 pellets were generously donated by Arkema, France. These pellets were used to make thin film substrates to simulate commercial balloon surfaces. Everolimus (EVE) ($C_{53}H_{83}NO_{14}$ MW 958.224 g/mol) and Mustang™ Percutaneous Transluminal Angioplasty (PTA) Balloon Dilatation Catheter were kindly provided by Boston Scientific Limited (Galway, Ireland). Pluronic P123 (P123) ($Mn \sim 5,800$) was purchased from Sigma Aldrich. All other reagents and chemicals used were of analytical grade.

2.2. PEBAX 7233 thin films as coating substrates

PEBAX 7233 thin films were used as a coating substrate for EVE-loaded P123. This PEBAX polymer is used as the outer surface of commercial drug-coated balloons (DCBs). The PEBAX 7233 thin films were prepared from pellets heated to 210°C using a heat press machine. 2 g polymer pellets were placed between thin Teflon sheets and these Teflon sheets were allowed to reach the set temperature and compressed at 200 bar for 5 *min*.

2.3. Sample preparation

PEBAX thin film specimens, used as balloon material, were coated with EVE-loaded P123 in various P123 to EVE ratios (Fig. 1). Initially, P123 and EVE were each dissolved in ethanol (EtOH) at a concentration of 10%(wt/v). These prepared formulations, with P123 to EVE ratios of 90 : 10, 75 : 25, and 50 : 50, were subsequently used to coat the balloon material samples via micro-pipetting. The target applied dose of EVE was consistently maintained at 3 $\mu g/mm2$ across all three formulations. The coated samples were then dried in a vacuum chamber overnight, at room temperature, and in the absence of light. Details of the different P123 and EVE formulations are presented in Table 1.

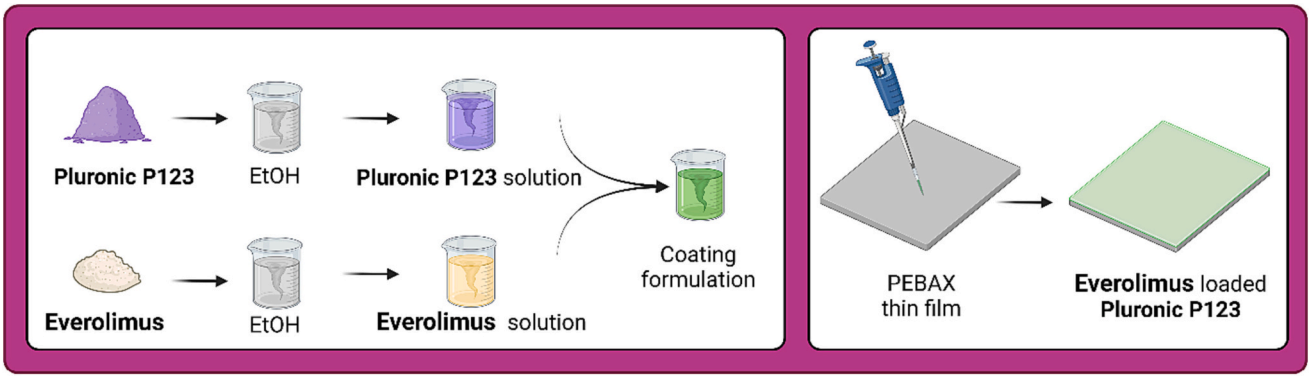

Fig. 1. Graphical representation for Everolimus-Loaded Pluronic P123 coating. Original image made with the online Biorender program.

Table 1
Pluronic P123 to Everolimus (wt/wt%), Pluronic P123 concentration (wt/vol%), Everolimus concentration (wt/vol%), weight of Pluronic P123 per mm^2 (μg), weight of Everolimus per mm^2 (μg), and the amount of formulation applied per cm^2 of PEBAX thin film (μl) used in the preparation of three different coating.

Pluronic P123: Everolimus (wt/wt%)	Initial Pluronic Concentration of P123 (wt/vol%)	Initial Concentration of Everolimus (wt/vol%)	Final Concentration of Pluronic P123 in the formulation (wt/vol%)	Final Concentration of Everolimus in the formulation (wt/vol%)	Weight of Pluronic P123 per mm^2 (μg)	Weight of Everolimus per mm^2 (μg)	Amount of formulation applied per cm^2 of PEBAX thin film (μl)
90 : 10	10	10	9	1	27	3	30
75 : 25	10	10	7.5	2.5	9	3	12
50 : 50	10	10	5	5	3	3	6

2.4. Microscopy observation

The surface of the different coatings and the pure drug powder was observed by a digital microscope (Keyence, VHX-7000) and scanning electron microscope (SEM, HITACHI S4800) at 2 kV energy. Before SEM measurement, the samples were sputter-coated for 15 s with 1 nm of Platinum.

2.5. Fourier transform infrared spectroscopy

A Thermo Scientific Nicolet iS50 FT-IR equipped with an attenuated total reflectance cell (ATR) was used to collect Fourier transform infrared spectroscopy (FTIR) spectra. In order to analyze the collected data, Thermo Scientific's OMNIC Series 8.2 software was used. All FTIR spectra were captured with scans ranging from 4000 to 750 cm^{-1}.

2.6. Differential scanning calorimetry

NETZSCH DSC200F3 calorimeters were used for the differential scanning calorimetry (DSC) examination. Thermal transitions of 10 mg of the sample were recorded between −20°C and 150°C at a rate of 10°C per minute in a perforated aluminum pan under a nitrogen purge.

2.7. Micelle formation characterization

P123 can form micelles in an aqueous solution. The critical micelle concentration (CMC) of P123 can vary from 25°C to 40°C approximately from 0.03 to 0.005%wt/v (Alexandridis et al., 1994). The formed micelles from the EVE-loaded P123 coatings were collected from the dispersed medium by centrifuging at 10, 000 rpm for 20 *min* for further characterization. The encapsulation efficiency (EE) and drug loading capacity (LC) were determined by using HPLC-UV at 277 nm. Both analyses were conducted in triplicate and determined by using the following equations (Eq. (1)), (Eq. (2)):

$$\%EE = \left(\frac{W_t - W_f}{W_t}\right) \times 100 \quad (1)$$

$$\%LC = \left(\frac{W_t - W_f}{W_m}\right) \times 100 \quad (2)$$

where"W_t" is the weight of the total actual amount of drug utilized in the micelles, the"W_f" is the amount of free drug examined in the supernatant, and the"W_m" is the total weight of micelles.

2.8. Dynamic light scattering

The size and size distribution of micelles were measured using the Nano ZS zetasizer system (Malvern Instruments). Measurement parameters were as follows: a scattering angle of 173°, a measurement temperature of 25°C, and at 37°C, a medium refractive index of 1.330. Before DLS measurement, the micelles were diluted in H_2O at a concentration of 1 mg/ml.

2.9. TEM analysis

Transmission electron microscopy (TEM) was carried out on a JEOL 1400 FLASH instrument, functioning at an acceleration voltage of 120 kV. To prepare the TEM samples, a 5 μl volume of the mixture was set on carbon-coated 300 mesh grids for one minute, then dried by making contact with absorbent paper. Subsequently, it was situated atop a droplet of a 2% uranyl acetate solution. After one minute, any surplus dye was gently eliminated by touching the periphery to absorbent paper, and the grid was left to dry under ambient conditions prior to examination.

2.10. HPLC-UV analysis

Chromatography was performed on HPLC-UV with the use of Kinetex™, 2.6 μm Phenyl-Hexyl; 2.1 × 50 mm (Phenomenex, Aschaffenburg, Germany) at 25°C temperature with a flow rate of 0.4 $mL.min^{-1}$. An isocratic elution method was employed in the analysis, in which a constant composition of the mobile phase was used throughout the analysis. The mobile phase consists of 20% of mobile phase A (mixture of 20 $mmol.L^{-1}$ ammonium formate in water +0.1%

formic acid) and 80% methanol as mobile phase B. EVE, the target compound, was detected with UV detection at 277 nm. A volume of 10 μL of a prepared sample was injected into the HPLC and a single run was completed in 10 *min*.

2.11. Drug release measurement from the coatings

The total amount of drug in the coating on the PEBAX thin film surface was quantified using the following method. Coated samples were immersed in 10 mL of PBS solution (10 mM, pH 7.4) and subjected to continuous horizontal shaking at 37°C, simulating body temperature, at a speed of 300 rpm for 1 *min*. The release of EVE was tracked over a span of 4 *min*, with measurements taken at 1 *min* intervals. At each time point, 1 ml of the release medium was removed to measure the quantity of EVE using HPLC-UV and replaced with fresh PBS. After 4 *min*, the samples were rinsed in 10 mL of EtOH to remove any residual EVE. The initial one-minute duration represents the tracking stage during the balloon angioplasty procedure, while the following three minutes simulate the deployment phase.

2.12. Balloon coating feasibility

Mustang™ Percutaneous Transluminal Angioplasty (PTA) Balloon Dilatation Catheter (Boston Scientific Limited, Galway, Ireland) was used for the EVE-loaded P123 coatings. Balloons were coated by a micro-pipetting method by keeping the target dose of EVE at 3 μg/mm2 across the whole coated area. The coated samples were then dried in a vacuum chamber overnight, at room temperature, and in the absence of light. The bare and coated balloon surface was observed by using ZEISS Stemi 508 Stereo Microscopes.

2.13. Statistical analysis

The statistical differences in the obtained results were evaluated using one-way ANOVA and Tukey's post hoc analysis via SPSS (IBM SPSS 25, USA). All data was depicted as mean values ± standard deviations, with differences considered significant at *p*-values below 0.05. All experiments were carried out three times.

3. Results and discussion

3.1. Morphology of the P123:EVE coatings on PEBAX

The digital microscopy and SEM analysis, Fig. 2, provided morphological characteristics of pure P123, and P123:EVE formulations in ratios of 90:10, 75:25, and 50:50, as well as the structure of the EVE powder. The pure P123 coating shows non-uniform and heterogeneous coating aspects throughout the surface. As the drug was introduced with

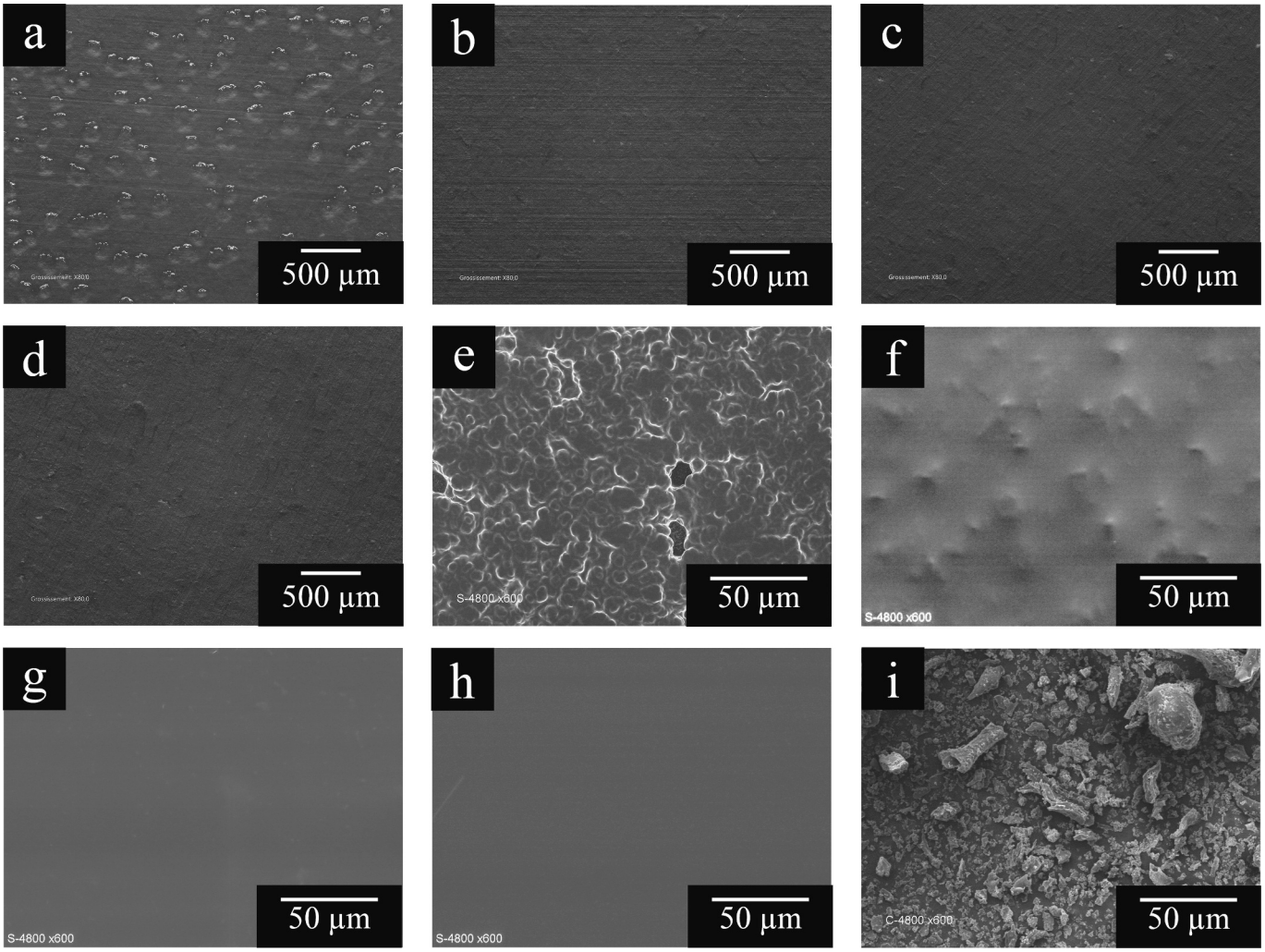

Fig. 2. Digital microscopy images of (a) Pure Pluronic P123 and various ratios of Pluronic P123: Everolimus (P123:EVE) (b) 90:10, (c) 75:25, and (d) 50:50. Scanning electron microscopy (SEM) images of (e) Pure Pluronic P123 and various ratios of Pluronic P123: Everolimus (f) 90:10, (g) 75:25, (h) 50:50 and (i) Everolimus Powder.

increasing ratios in the P123, the surface quality of the film started to increase in homogeneity. The 90:10 formulation presented a more complete surface coverage than the pure P123, despite some visible asperities. For the 75:25 and the 50:50 ratios, surface homogeneity was more obvious, and smooth surface coverage can be observed. This behavior points to better surface coverage as the drug ratio increases. The introduction of the hydrophobic drug allows better interaction of the formulation with the hydrophobic PEBAX surface thus favoring spreadability and surface coverage. Indeed, no phase separation or visible drug particles are seen on the microscopy images with these two formulations. The absence of distinctly visible drug particles in all the formulations suggests that the EVE was maintained dispersed into the P123 matrix, with no crystallization or agglomeration of drug molecules. This is an indication of good miscibility between the drug molecules and the P123 polymer matrix.

The morphological characteristics of the P123:EVE coatings on PEBAX, as revealed in our study, are significant in advancing DCB technology. Our findings demonstrate an improvement in uniformity and surface coverage which directly addresses the challenges faced by drug-eluting stents (DES). In DES, non-uniform drug distribution is a notable drawback, leading to higher concentrations at stent struts and lower in between, potentially increasing risks of inflammation, delayed endothelialization, and thrombosis (Dash et al., 2022), (Cortese and Bertoletti, 2012). In contrast, the enhanced homogeneity in DCBs, as shown in our results, aligns with the objective of maintaining effective local drug concentrations to counteract the hyperproliferative response to vascular injury (Tesfamariam, 2016).

3.2. EVE dispersion in P123 determined by FTIR and DSC

Fig. 3 shows the Fourier Transform Infrared (FTIR) spectra of Pure P123, and various ratios of P123: EVE and EVE powder. The P123-related stretching modes are associated with the peaks at 2970 cm^{-1} (asymmetric CH_2 stretching), 2871 cm^{-1} (symmetric CH_2 stretching), 1465 cm^{-1} (-C-O-C- stretching vibrations), 1343 cm^{-1} (bending vibrations of -C-H), and 1100 cm^{-1} (-C-O-C-vibration) (Ulu et al., 2022). In the case of the FTIR spectra of EVE, peaks at 3416 cm^{-1}, 2930 cm^{-1}, 1642 cm^{-1}, 1449 cm^{-1}, and 989 cm^{-1}corresponding to -O-H stretching vibrations, (-CH3), (C=O), (-C-O-C-), and out-of-plane -C-H bending vibrations in -CH=CH- bonds, respectively (Maki et al., 2019), (Zhang et al., 2022). As the concentration of EVE increases, the corresponding peaks (989, 1642, 1718, 3416 cm^{-1}) strengthen coherence with the composition. Similarly, a decrease in the intensity of the 2871 cm^{-1}peak is seen as the concentration of P123 decreases diminishing the contribution from the P123 functional groups. As no significant shifts or new peaks are introduced and there is a consistency of peak positions and the relative increase or decrease in peak intensity with the change in ratios, it is possible to put forward that P123 and EVE do not specifically interact together. Their molecular structures and functional group vibrations are maintained.

As shown in the thermograms of Fig. 4, for pure P123, a melting point at 36°C consistent with the literature is observed (Song et al., 2010), (Ahmed et al., 2021). EVE demonstrated a glass transition temperature of 82.5°C consistent with its amorphous structure and as reported previously (Ma et al., 2020), (Wyttenbach and Kuentz, 2017). The DSC results for the different P123 to EVE formulations (90:10, 75:25, 50:50) exhibit a downward shift in the melting temperatures compared to the pure P123. The 90:10 and 75:25 formulations exhibit a melting peak at 31.5°C and 29°C, respectively. The lowering of the melting point in the 90:10 and 75:25 formulations compared to pure P123 can be attributed to the disruption of the crystalline structure of P123 due to the incorporation of EVE. This can indicate a good degree of miscibility between P123 and EVE in these formulations. Furthermore, the 50:50 formulation does not display a discernible melting point leaning toward the hypothesis of good miscibility and P123 crystallinity inhibition by the EVE molecules. These observations are coherent with

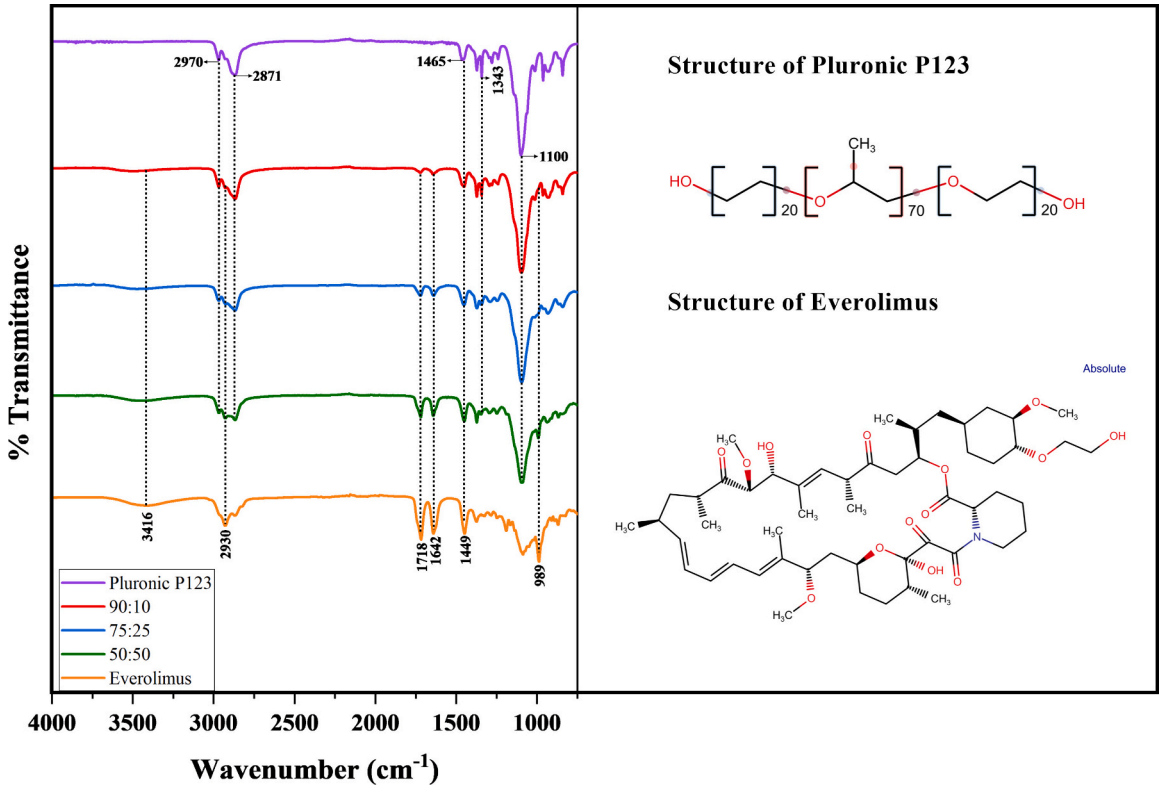

Fig. 3. Fourier transform infrared (FTIR) spectrum of Pure Pluronic P123, various ratios of Pluronic P123: Everolimus (P123:EVE), 90:10, 75:25, 50:50 and Everolimus powder.

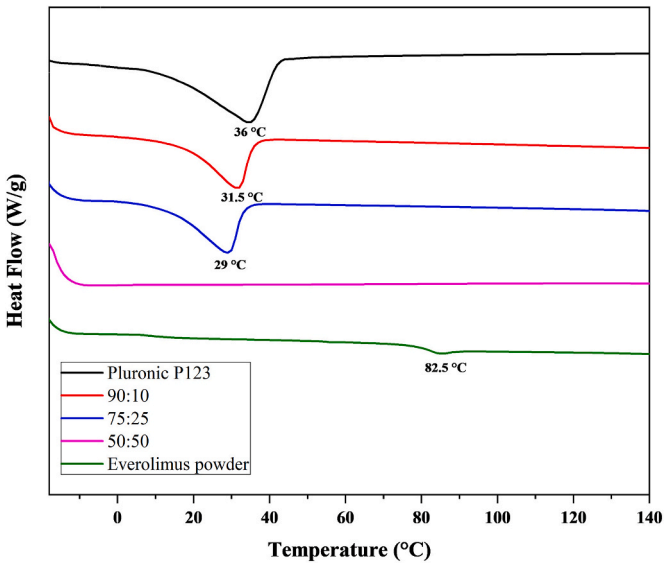

Fig. 4. Differential Scanning Calorimetry (DSC) of Pure Pluronic P123, various ratios of Pluronic P123: Everolimus (P123:EVE), 90:10, 75:25, 50:50 and Everolimus powder.

the explanations of the increased smoothness and coating homogeneity observed by SEM. The transition to an amorphous state raises important considerations in the context of drug-coated balloon (DCB) technology. While crystalline coatings are recognized for providing higher tissue levels and prolonged drug retention, their brittleness and potential fragility can lead to challenges. According to previous studies, the advantageous use of amorphous coatings in DCBs stems from their ability to offer more uniform balloon coverage and reduced risk of particulate generation during balloon inflation, a significant consideration for patient safety and the efficacy of drug delivery (Gongora et al., 2015), (Tesfamariam, 2016). Furthermore, the crystalline form of drugs like paclitaxel, though effective in retaining drugs within the arterial wall, can lead to greater risks of distal embolization and related complications (Caradu et al., 2019), (van den Berg, 2017). Amorphous coatings, as our study suggests, may offer a safer alternative with higher solubility and a lower propensity for particulate embolization, albeit with traditionally reduced stability (Woolford et al., 2019), (Heinrich et al., 2020). Our research contributes to this ongoing discussion in the field of DCB technology. The transition toward an amorphous structure in our coatings may offer a more balanced approach in terms of safety and efficacy, aligning with the evolving needs for drug coatings that not only ensure effective drug transfer and retention but also prioritize patient safety.

3.3. Study of loading capacity (LC) and encapsulation efficiency (EE) in Everolimus loaded Pluronic P123 self-assembled micelles

EVE-loaded P123 micelles were fabricated by the thin-film hydration method (Sahu et al., 2011). Fig. 5 (a and b) indicates the schematic representation of micelles formation from coatings and the results of the drug loading capacity (LC) and encapsulation efficiency (EE) percentages of micelle formulations of P123 and EVE in the ratios of 90:10, 75:25, and 50:50. Regarding the drug loading capacity (LC), for the 90:10 formulation, the LC was measured to be 5.12 ± 0.78%. The LC markedly improved to 16.31 ± 2.46% and the highest LC was noted with the 50:50 formulation, at 38.36 ± 1.39%. This sequential increase

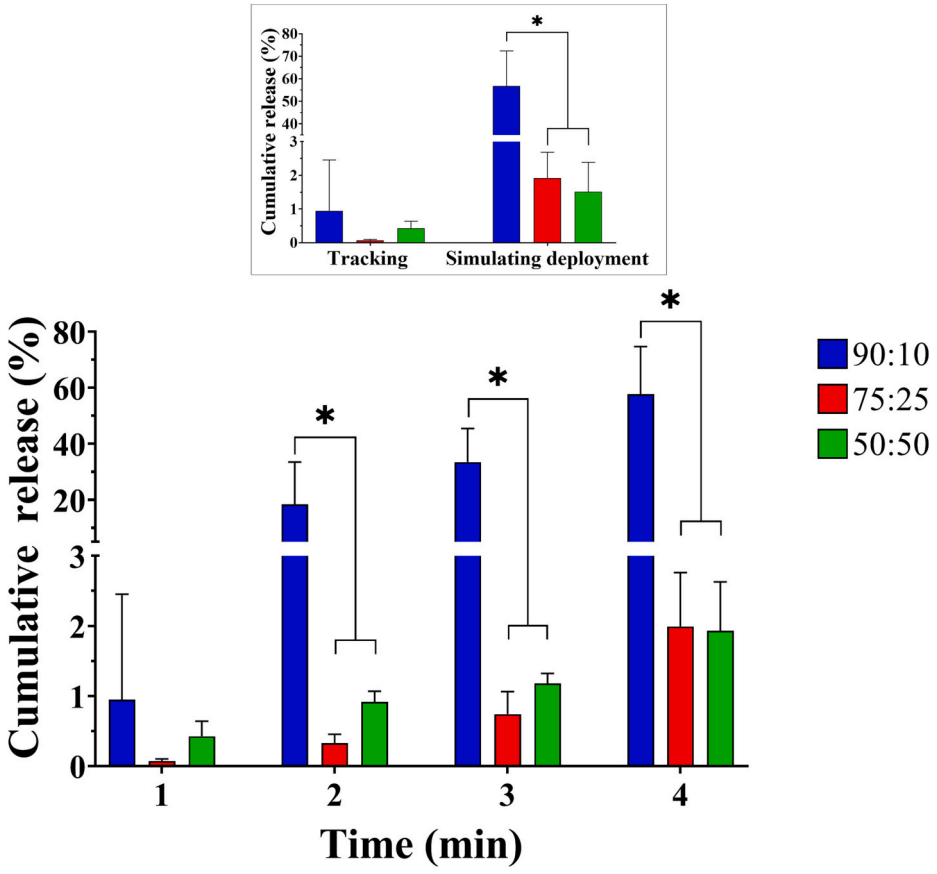

Fig. 5. (a) Schematic representation of micelles formation from coatings, original image made with the online Biorender program, (b) drug encapsulation efficiency (EE%), and drug loading capacity (LC%) of various ratios of Pluronic P123: Everolimus (P123:EVE), 90:10, 75:25, and 50:50, (c and d) Average micelle size and polydispersity (PDI) of Pure Pluronic P123, various ratios of Pluronic P123: Everolimus (P123:EVE), 90:10, 75:25, and 50:50.

in LC with an increase in EVE content suggests a direct relationship between the EVE content and the micelles' drug-loading capacity. This is potentially due to the enhanced hydrophobic interactions between EVE and the P123 micelle core, which enables more efficient drug loading. In terms of encapsulation efficiency (EE), the 90:10 formulation achieved an EE of 48.61 ± 7.83%. The EE rose to 58.68 ± 10.38% in the 75:25 formulation and further to 62.28 ± 3.65% in the 50:50 formulation. The incremental increase in EE with increasing EVE content could be attributed to the increased hydrophobicity with higher EVE percentages. This increased hydrophobicity enhances the interaction between EVE and the micellar core, leading to better drug encapsulation.

3.4. DLS Analysis of Everolimus loaded Pluronic P123 self-assembled micelles

Fig. 5 (c and d) show the experimental results obtained from Dynamic Light Scattering (DLS) provide information about the size and polydispersity index (PDI) of micelles formed from pure P123 and the different formulations with EVE at different ratios (90:10, 75:25, 50:50). These measurements were conducted at two distinct temperatures, 25 °C and 37 °C, which mimic ambient and physiological conditions, respectively. At 25 °C, the size of pure P123 micelles was measured to be 18.52 ± 0.03 nm with a PDI of 0.03 ± 0.01. This indicates small, homogeneous micelles. However, as the proportion of EVE was increased in the formulation, both the size of the micelles and their PDI increased. The 90:10 formulation produced micelles with a size of 54.68 ± 0.70 nm and a PDI of 0.31 ± 0.01. Further increase in EVE concentration to the 75:25 ratio resulted in even larger micelles with a size of 88.45 ± 0.36 nm and a PDI of 0.33 ± 0.03. Finally, the 50:50 formulation resulted in the largest micelles with a size of 123.20 ± 2.954 nm and a PDI of 0.22 ± 0.01. This trend implies that as the EVE concentration increased, the size of the micelles became larger and more heterogeneous. At physiological temperature (37 °C), a similar trend was observed. The size of pure P123 micelles slightly increased to 20.84 ± 1.19 nm, and their PDI marginally reduced to 0.02 ± 0.01. As the EVE concentration increased, the size of the micelles generally grew. The 90:10, 75:25, and 50:50 formulations resulted in micelles of size 61.27 ± 3.30 nm, 100.60 ± 2.28 nm, and 116.40 ± 4.27 nm, respectively. The increase in micelle size with increasing EVE concentration could be attributed to the hydrophobic interactions between the EVE and the PPO core of the P123, leading to the formation of larger micelle structures. This seems to be in correlation with LC and EE in which more drugs are encapsulated as the drug concentration rises. The increase in PDI with increasing EVE concentration suggests increased heterogeneity in the micelle size distribution, likely due to differing degrees of incorporation of EVE into the micelles.

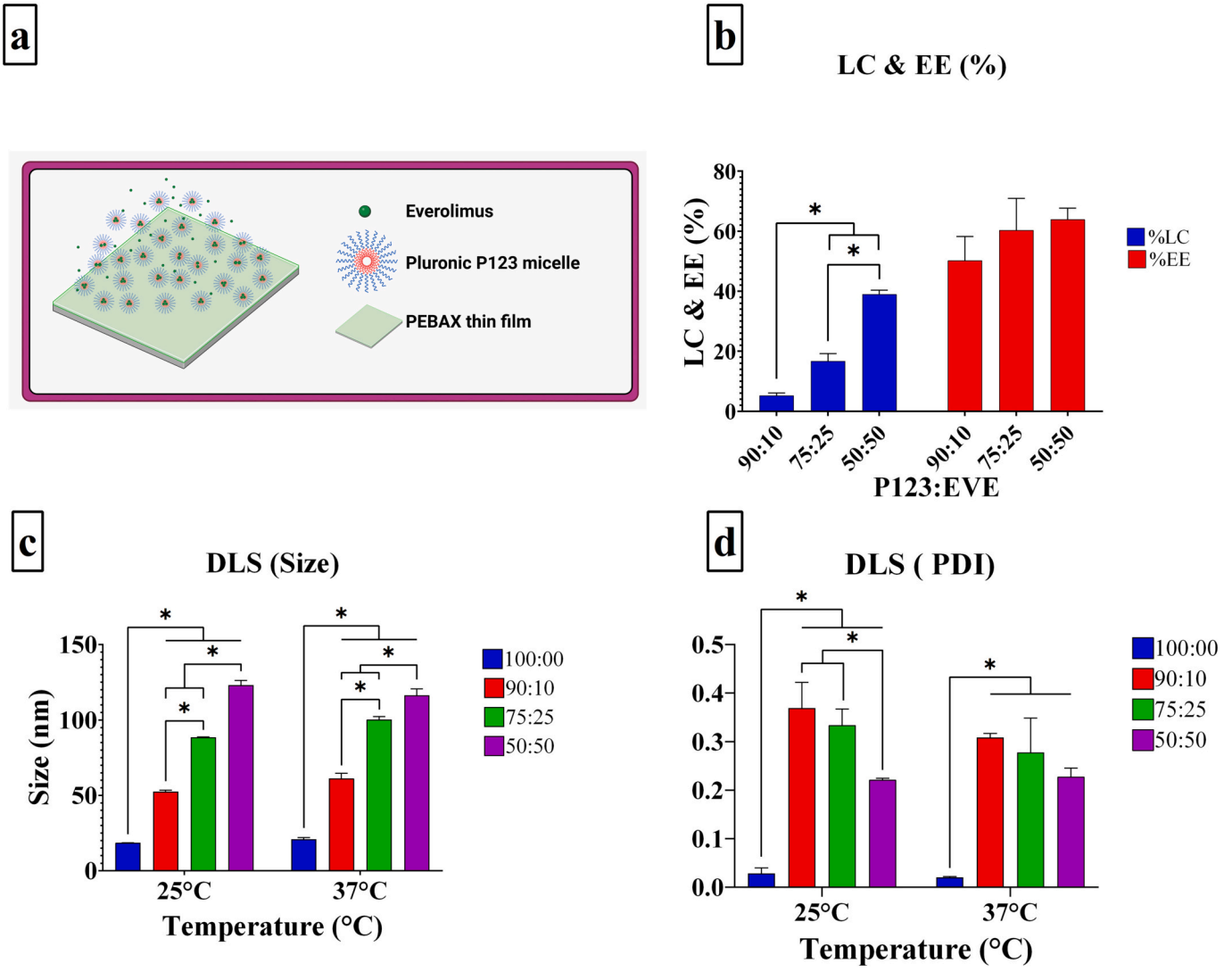

Fig. 6. Transmission electron microscopes (TEM) and micelle size distribution curve of (a) Pure Pluronic P123 and various ratios of Pluronic P123: Everolimus (P123:EVE), (b) 90:10, (c) 75:25, and (d) 50:50.

3.5. TEM Analysis of Everolimus loaded Pluronic P123 self-assembled micelles

Fig. 6 shows the experimental results obtained through Transmission electron microscopy (TEM) and particle size distribution curve of the micelles formed from P123, and its formulations with EVE at various ratios: 90:10, 75:25, and 50:50. For pure P123, the average micelle size was found to be 29.10 ± 6.97 nm. This indicates the small size of the micelles formed solely by the P123 copolymer. However, the inclusion of EVE impacted the size of the resultant micelles. The 90:10 P123 to EVE formulation resulted in a significantly larger micelle size, averaging 84.50 ± 16.42 nm. Upon further increasing the EVE amount in 75:25 and 50:50 formulations, there is a slight decrease in micelle size to 77.66 ± 17.66 nm and 74.67 ± 16.29 nm, respectively. The different sizes observed in TEM images compared to dynamic light scattering may be due to the drying effect during sample preparation for TEM measurements (Tang et al., 2019).

3.6. In vitro EVE release studies

DCB treatment for vascular conditions consists of two main phases after introduction into the vasculature: tracking and deployment. During the tracking, the undeflated drug-coated balloon navigates the vascular system from the insertion site to the target lesion site; During this phase, one requirement of the DCB is to avoid drug loss in the bloodstream. After reaching the lesion site, deployment can occur. During deployment, the DCB is inflated and the drug should be delivered to the lesion tissue and its surroundings at therapeutic dosages (Woolford et al., 2022). The standard curve of EVE was obtained through EVE solutions in a concentration gradient ($y = 66682x + 4139$, $R2 = 0.9990$), where y and x correspond to absorbance and EVE concentration ($\mu g.mL^{-1}$), respectively. Fig. 7 indicates the release profiles of EVE from P123 coatings with different P123:EVE ratios (90 : 10, 75 : 25, 50 : 50). The release was evaluated over a span of 4 min (1-min intervals), representing the tracking and deployment phases of a DCB angioplasty procedure. During the tracking phase (first minute), the 90 : 10 formulation showed the highest release (0.95 ± 1.51%), followed by the 75 : 25 (0.07 ± 0.03%) and 50 : 50 (0.42 ± 0.22%) formulations. The increased initial release in the 90 : 10 formulation may be due to the larger proportion of P123 on the surface of the coating, leading to a higher initial release. Particulate generation downstream has been a safety concern since the inception of first-generation DCBs due to coating matrices separating from the DCB surface during tracking and inflation. Optimal coatings resist cracking and delamination upon inflation, while factors like improper storage and manufacturing can also cause delamination (Xiong et al., 2016), (Huang et al., 2023). Notably, using P123 as a coating has effectively minimized drug loss during the simulated tracking time. Upon simulating deployment over the next three minutes, the 90 : 10 formulation also exhibited the greatest release (56.78 ± 15.57%), whereas the 75 : 25 and 50 : 50 formulations showed lower release (1.92 ± 0.76% and 1.51 ± 0.88% respectively). This suggests that a higher proportion of P123 in the coating matrix might lead to a more efficient delivery of the therapeutic agent at the site of action. The lower release rates for the 75 : 25 and 50 : 50 formulations during the deployment phase (1.92 ± 0.76% and 1.51 ± 0.88% respectively) are due to the higher proportion of EVE, and thus a more hydrophobic formulation. The cumulative release over the 4-min duration increased with time for all formulations, with the highest release observed for the 90 : 10 formulation (57.72 ± 16.97%), followed by the 75 : 25 formulations (1.99 ± 0.77%), and the 50 : 50 (1.93 ± 0.70%). The results suggest that the ratio of P123 to EVE impacts the drug release characteristics during both the tracking and deployment phases. While our study primarily models the peripheral artery context, the 4-min timeframe for drug release, as derived from (Woolford et al., 2022), should be interpreted with caution for coronary applications. According to (Byrne et al., 2014), shorter balloon inflation times are recommended for coronary arteries (30–60 s) compared to peripheral arteries (up to 180 s). Our findings are in alignment with the study by (Woolford et al., 2022), which indicates that increased excipient amounts in the coating composition enhance drug release under physiological conditions.

The P123 coating developed for this study is designed to function as a vehicle for delivering EVE-loaded self-assembled micelles directly to the lesion area. This aligns with the findings from the DLS and TEM analyses (Sections 3.4 and 3.5 respectively), which confirm that Pluronic forms micelles in an aqueous environment. These micelles are likely to facilitate a sustained, slow release of the drug at the lesion site, thereby potentially enhancing the treatment's efficacy.

The release mechanism of the drug from these polymeric micelles is primarily attributed to two processes: drug diffusion from intact micelles and micelle disassembly (Ghezzi et al., 2021). Additionally, incorporating the insights regarding the micelle internalization pathways into our discussion of the in vitro EVE release studies provides a deeper understanding of the potential mechanisms at play in our novel DCB coating methodology. As highlighted in previous studies (Nelemans and Gurevich, 2020), (Maysinger et al., 2007), (Ghezzi et al., 2021), micelles have a pivotal role in delivering drugs to specific targets at a subcellular level, with endocytosis being the main pathway for their internalization. This involves the micelle interaction with the cellular membrane, followed by its uptake into cells, and transport within endosomes to ultimately reach the cell's cytoplasm. The self-assembled EVE-loaded P123 micelles are likely to interact with cellular membranes and undergo similar internalization processes. It has been found that polymeric micelles often disassemble at the plasma membrane or degrade within lysosomes (Maysinger et al., 2007), which could have implications for how EVE is released at the target site. This disassembly could lead to the release of the drug either inside or outside the cells, potentially in disaggregated unimer forms, resulting in drug accumulation in various cellular compartments (Lee et al., 2013), (Cui et al., 2013), (Ghezzi et al., 2021). This behavior is critical to consider, as it might influence the efficacy of EVE delivery to the lesion tissue during the deployment phase of DCB treatment.

Furthermore, this approach to drug delivery finds resonance with previous studies in the field. Notably, Lemos et al. (Lemos et al., 2013), conducted a seminal study revealing that sirolimus-loaded nano-carriers, delivered via a coronary stent-plus-balloon system or a standalone balloon, were effective in transferring the drug throughout all layers of the arteries. Following this line of research, nanoparticle eluting balloons have demonstrated a remarkable capacity for both maximizing local drug delivery and achieving sustained in vitro drug release (Iyer et al., 2019). This is particularly pertinent to our study as it underscores the potential of nano-carriers, akin to our micelles, in enhancing drug delivery efficiency. The implication here is that our coating, through its innovative use of micelles, could potentially offer similar benefits in terms of targeted and effective drug distribution within arterial regions.

3.7. Coating efficiency onto the angioplasty balloon

The Mustang™ PTA Balloons were used for applying EVE-loaded P123 coatings, with a target dose of EVE at 3 μg/mm^2 over the entire coated surface. The coating was done using the micro-pipetting method (Supplementary Video 1). Micro-pipetting brings several benefits including uniformity and precise control over the application, distinct placement of the drug/excipient solution in pockets underneath folds, and total control over the dose (Xiong et al., 2016).

Fig. 8 shows the homogenous surface coating of the balloon. The coating applied on the balloon covered the whole surface of the balloon which could be effective for uniform drug transfer toward the arterial wall.

Considering the drug release aspect, the non-compliant nature of the balloon material used in our study plays a crucial role. Non-compliant

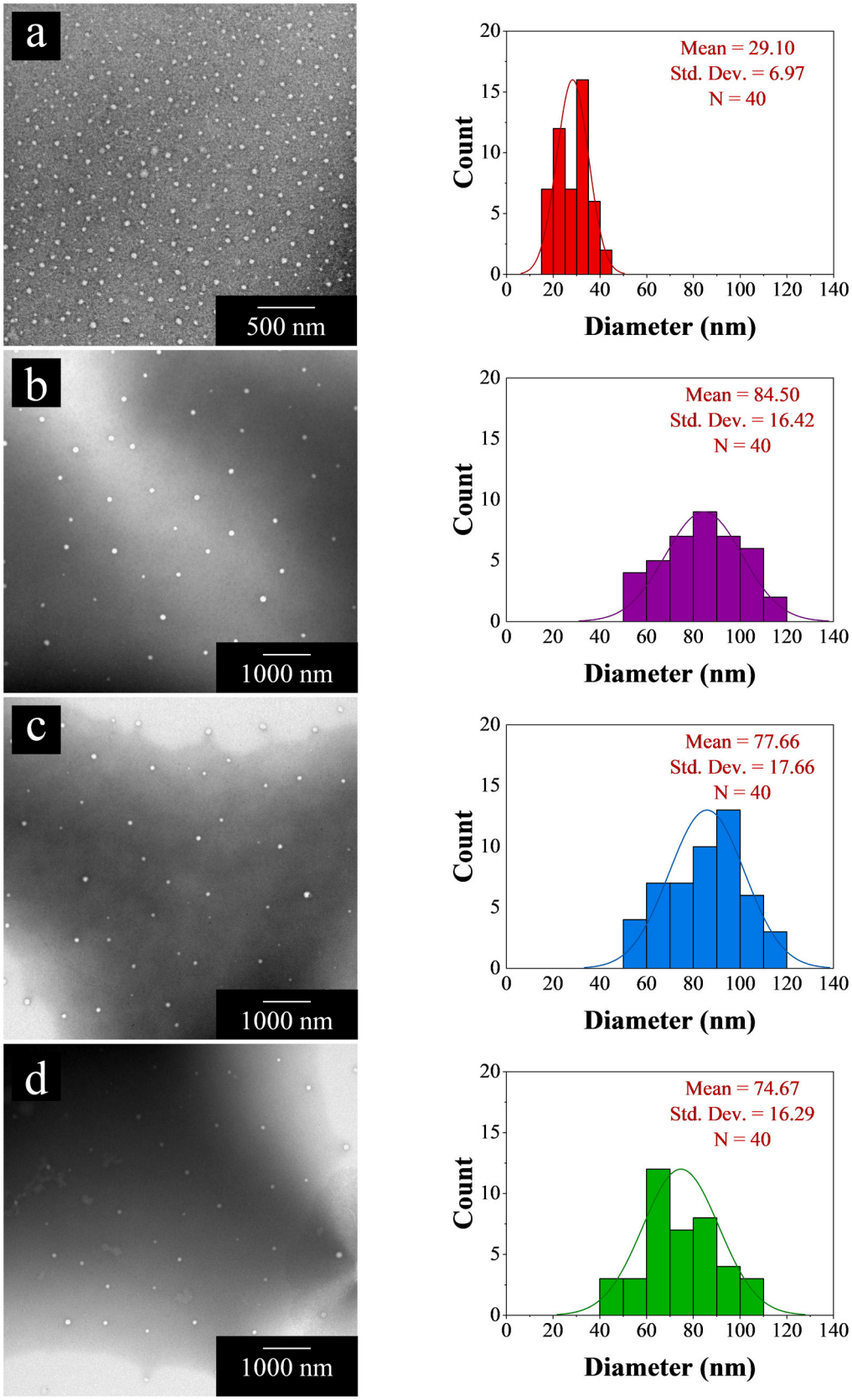

Fig. 7. Everolimus release profile of various ratios of Pluronic P123: Everolimus (P123:EVE), 90:10, 75:25, and 50:50. Insert within Fig. 7 shows the amount of Everolimus release during the tracking and simulating deployment.

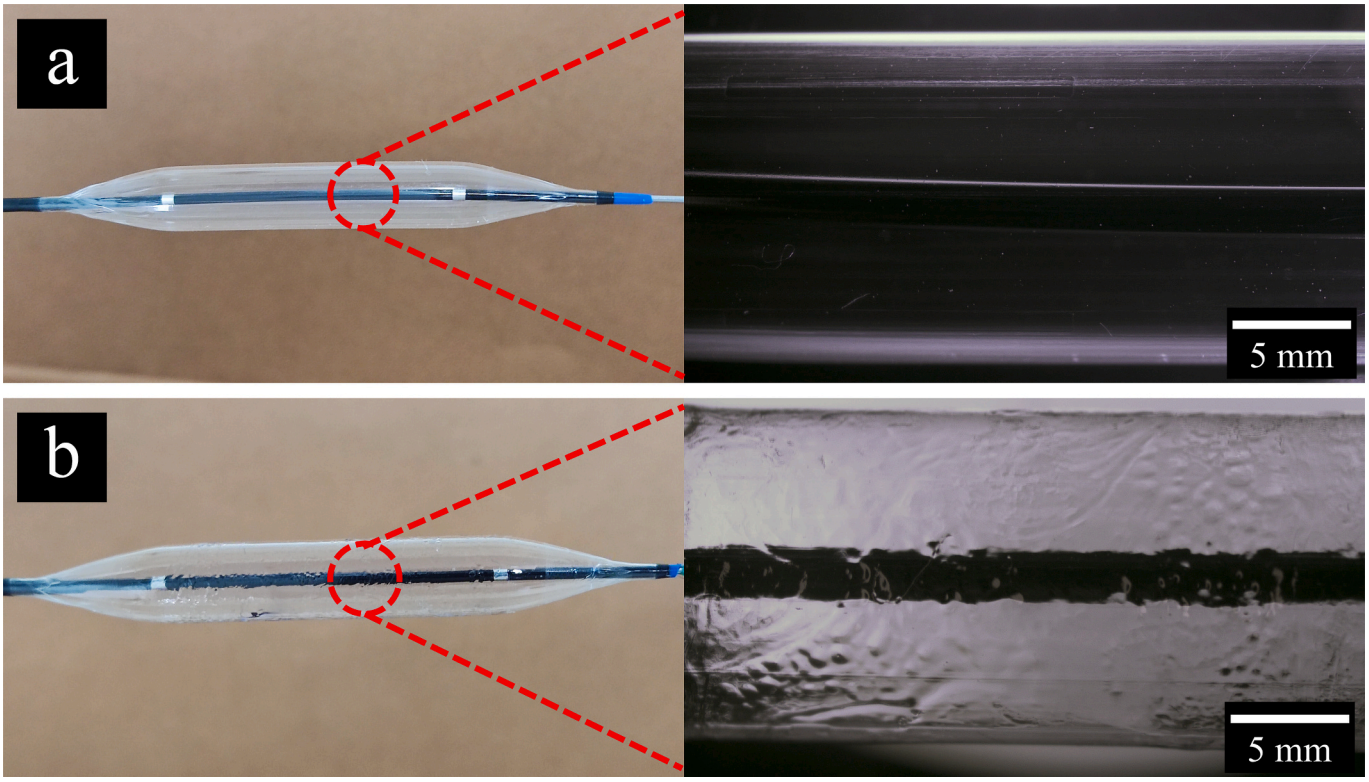

Fig. 8. Picture and Stereo Microscopes image of Mustang™ Percutaneous Transluminal Angioplasty (PTA) Balloon Dilatation Catheter (a) uncoated inflated balloon, and (b) coated inflated balloon with EVE-loaded P123 with a ratio of 90:10.

balloons are designed to maintain their shape and size under pressure, leading to a minimal increase in surface area upon inflation. According to the balloon's Directions for Use, in our case, the diameter varies from 9.97 mm to 10.34 mm when inflated between 8 atm and 14 atm, the rated pressure. This translates to only a 3.71% increase in surface area for a 40 mm balloon if deployed at the rated pressure. Therefore, the impact of inflation on drug release in our study is considerably less than what might be observed with compliant or semi-compliant balloons. This minimal change in surface area may suggest the applicability of our drug release studies conducted on coated thin films. Although these films were not directly characterized for similarity, they could provide an initial insight into the potential behavior of drug release from the actual balloon surface in practical applications.

4. Summary

This study investigated the feasibility of using different P123:EVE coating ratios, for a micellization release of antiproliferative drugs from DCBs. Polymeric micelles, which self-assemble into a hydrophilic shell and hydrophobic core, are highly suited for delivering hydrophobic drugs such as EVE. The microscopy images, FTIR, and DSC results showed that the P123:EVE coatings were homogeneous and the EVE was molecularly dispersible and miscible in the P123 matrix. The DSC findings in our study are further contextualized by literature indicating that while crystalline drug forms ensure better retention in the arterial wall, they also pose a higher risk of distal embolization and downstream tissue necrosis. In contrast, amorphous forms provide more uniform coverage and lower toxicity, aligning with our observations of the P123:EVE coatings. These findings highlight the importance of achieving a balance between acute drug transfer and long-term tissue retention, which our P123:EVE micelle formulations aim to optimize. Additionally, DCBs often face significant drug loss in the bloodstream during balloon tracking, resulting in sub-therapeutic levels at the treatment site. However, our drug release studies indicated that with <1% drug loss in the tracking phase, the 90:10 P123:EVE formulation excelled in drug release during deployment, suggesting its efficacy in therapeutic delivery. The micellization study demonstrated that with an increase in the content of EVE in the P123:EVE formulation, both the LC and EE of the assembled micelles also increased, attributed to stronger hydrophobic interactions. DLS and TEM analysis indicated that increasing EVE proportion also led to an increase in micelle size. Finally, the study showed proof of concept feasibility by coating commercial balloons. The results showed a homogeneous coating over the entire balloon surface, thereby potentially promoting uniform drug transfer to the arterial wall. In conclusion, this study demonstrates the potential use of P123 as an alternate micellization drug delivery platform for drug-coated balloons.

Supplementary data to this article can be found online at https://doi.org/10.1016/j.ijpx.2024.100230.

CRediT authorship contribution statement

Mohammad Akrami-Hasan-Kohal: Conceptualization, Formal analysis, Investigation, Methodology, Writing – original draft, Writing – review & editing, Visualization. **Adrien Chouchou:** Methodology, Writing – review & editing. **Sébastien Blanquer:** Writing – review & editing, Supervision. **Tahmer Sharkawi:** Conceptualization, Funding acquisition, Project administration, Resources, Supervision, Writing – review & editing, Methodology.

Declaration of competing interest

The authors declare that they have no known competing financial interests or personal relationships that could have appeared to influence the work reported in this paper.

Data availability

Data will be made available on request.

Acknowledgments

This project has received funding from the European Union's Horizon 2020 research and innovation program under grant agreement No 956470.

References

Abbott, J.D., Wykrzykowska, J.J., Lenselink, C., 2023. Drug-coated balloons in small vessels: preferred strategy to drug-eluting stents?*. J. Am. Coll. Cardiol. Intv. 16, 1062–1064.
Ahmed, S., Kassem, M.A., Sayed, S., 2021. Co-polymer mixed micelles enhanced transdermal transport of Lornoxicam: in vitro characterization, and in vivo assessment of anti-inflammatory effect and antinociceptive activity. J. Drug Deliv. Sci. Technol. 62, 102365.
Akhmetzhan, G., Olaifa, K., Kitching, M., Cahill, P.A., Pham, T.T., Ajunwa, O.M., Marsili, E., 2023. Biochemical and electrochemical characterization of biofilms formed on everolimus-eluting coronary stents. Enzym. Microb. Technol. 163, 110156.
Alexandridis, P., Holzwarth, J.F., Hatton, T.A., 1994. Micellization of poly(ethylene oxide)-poly(propylene oxide)-poly(ethylene oxide) triblock copolymers in aqueous solutions: thermodynamics of copolymer association. Macromolecules 27, 2414–2425.
Ali, R.M., Abdul Kader, M.A.S.K., Wan Ahmad, W.A., Ong, T.K., Liew, H.B., Omar, A.-F., Mahmood Zuhdi, A.S., Nuruddin, A.A., Schnorr, B., Scheller, B., 2019. Treatment of coronary drug-eluting stent restenosis by a sirolimus- or paclitaxel-coated balloon. J. Am. Coll. Cardiol. Intv. 12, 558–566.
Anderson, J.A., Lamichhane, S., Remund, T., Kelly, P., Mani, G., 2016. Preparation, characterization, in vitro drug release, and cellular interactions of tailored paclitaxel releasing polyethylene oxide films for drug-coated balloons. Acta Biomater. 29, 333–351.
Ang, H., Lin, J., Huang, Y.Y., Chong, T.T., Cassese, S., Joner, M., Foin, N., 2018. Drug-coated balloons: technologies and clinical applications. Curr. Pharm. Des. 24, 381–396.
Anirudhan, T.S., Varghese, S., Manjusha, V., 2021. Hyaluronic acid coated Pluronic F127/Pluronic P123 mixed micelle for targeted delivery of Paclitaxel and Curcumin. Int. J. Biol. Macromol. 192, 950–957.
Batrakova, E.V., Kabanov, A.V., 2008. Pluronic block copolymers: evolution of drug delivery concept from inert nanocarriers to biological response modifiers. J. Control. Release 130, 98–106.
Byrne, R.A., Joner, M., Alfonso, F., Kastrati, A., 2014. Drug-coated balloon therapy in coronary and peripheral artery disease. Nat. Rev. Cardiol. 11, 13–23.
Cai, H., Dong, J., Ye, Y., Song, Q., Lu, S., 2022. Safety and efficacy of drug-coated balloon in the treatment of below-the-knee artery: a meta-analysis. J. Surg. Res. 278, 303–316.
Caradu, C., Lakhlifi, E., Colacchio, E.C., Midy, D., Bérard, X., Poirier, M., Ducasse, E., 2019. Systematic review and updated meta-analysis of the use of drug-coated balloon angioplasty versus plain old balloon angioplasty for femoropopliteal arterial disease. J. Vasc. Surg. 70, 981–995.e910.
Cortese, B., Bertoletti, A., 2012. Paclitaxel coated balloons for coronary artery interventions: a comprehensive review of preclinical and clinical data. Int. J. Cardiol. 161, 4–12.
Cortese, B., Di Palma, G., Guimaraes, M.G., Piraino, D., Orrego, P.S., Buccheri, D., Rivero, F., Perotto, A., Zambelli, G., Alfonso, F., 2020. Drug-coated balloon versus drug-eluting stent for small coronary vessel disease: PICCOLETO II randomized clinical trial. J. Am. Coll. Cardiol. Intv. 13, 2840–2849.
Cui, C., Xue, Y.-N., Wu, M., Zhang, Y., Yu, P., Liu, L., Zhuo, R.-X., Huang, S.-W., 2013. Cellular uptake, intracellular trafficking, and antitumor efficacy of doxorubicin-loaded reduction-sensitive micelles. Biomaterials 34, 3858–3869.
Dash, D., Mody, R., Ahmed, N., Malan, S.R., Mody, B., 2022. Drug-coated balloon in the treatment of coronary bifurcation lesions: a hope or hype? Indian Heart J. 74, 450–457.
Escuer, J., Schmidt, A.F., Peña, E., Martínez, M.A., McGinty, S., 2022. Mathematical modelling of endovascular drug delivery: balloons versus stents. Int. J. Pharmaceut. 620, 121742.
Ghezzi, M., Pescina, S., Padula, C., Santi, P., Del Favero, E., Cantù, L., Nicoli, S., 2021. Polymeric micelles in drug delivery: an insight of the techniques for their characterization and assessment in biorelevant conditions. J. Control. Release 332, 312–336.
Giacoppo, D., Alfonso, F., Xu, B., Claessen, B.E.P.M., Adriaenssens, T., Jensen, C., Pérez-Vizcayno, M.J., Kang, D.-Y., Degenhardt, R., Pleva, L., Baan, J., Cuesta, J., Park, D.-W., Kukla, P., Jiménez-Quevedo, P., Unverdorben, M., Gao, R., Naber, C.K., Park, S.-J., Henriques, J.P.S., Kastrati, A., Byrne, R.A., 2020. Drug-coated balloon angioplasty versus drug-eluting stent implantation in patients with coronary stent restenosis. J. Am. Coll. Cardiol. 75, 2664–2678.
Giacoppo, D., Saucedo, J., Scheller, B., 2023. Coronary drug-coated balloons for De Novo and in-stent restenosis indications. J. Soc. Cardiovasc. Angiography Interv. 100625.
Gongora, C.A., Shibuya, M., Wessler, J.D., McGregor, J., Tellez, A., Cheng, Y., Conditt, G. B., Kaluza, G.L., Granada, J.F., 2015. Impact of paclitaxel dose on tissue pharmacokinetics and vascular healing: a comparative drug-coated balloon study in the familial hypercholesterolemic swine model of superficial femoral in-stent restenosis. J. Am. Coll. Cardiol. Intv. 8, 1115–1123.
Heinrich, A., Engler, M.S., Güttler, F.V., Matthäus, C., Popp, J., Teichgräber, U.K.M., 2020. Systematic evaluation of particle loss during handling in the percutaneous transluminal angioplasty for eight different drug-coated balloons. Sci. Rep. 10, 17220.
Huang, L., Fang, H., Zhang, T., Hu, B., Liu, S., Lv, F., Zeng, Z., Liu, H., Zhou, W., Wang, X., 2023. Drug-loaded balloon with built-in NIR controlled tip-separable microneedles for long-effective arteriosclerosis treatment. Bioact. Mater. 23, 526–538.
Iyer, R., Kuriakose, A.E., Yaman, S., Su, L.-C., Shan, D., Yang, J., Liao, J., Tang, L., Banerjee, S., Xu, H., Nguyen, K.T., 2019. Nanoparticle eluting-angioplasty balloons to treat cardiovascular diseases. Int. J. Pharmaceut. 554, 212–223.
Jebari-Benslaiman, S., Galicia-García, U., Larrea-Sebal, A., Olaetxea, J.R., Alloza, I., Vandenbroeck, K., Benito-Vicente, A., Martín, C., 2022. Pathophysiology of Atherosclerosis, 23, p. 3346.
Jumat, M.A., Chevallier, P., Mantovani, D., Saidin, S., 2022. Everolimus immobilisation using polydopamine intermediate layer on poly(l-lactic acid)/poly(d-lactic acid) scaffold for sustainable anti-proliferative drug release. Mater. Today Commun. 31, 103720.
Kasbaoui, S., Payot, L., Zabalawi, A., Delaunay, R., Amara, W.B., Boukhris, M., Taldir, G., 2023. Safety and efficacy of a hybrid approach combining a paclitaxel-coated balloon with a new generation drug-eluting stent in patients with de novo true coronary bifurcation lesions. Cardiovasc. Revasc. 54, 47–56.
Kouser Qadri, H., Shaheen, A., Rashid, S., Ahmad Bhat, I., Mohammad Rather, G., Ahmad Dar, A., 2022. Micellization and gelation characteristics of Pluronic P123 and single ester-bonded cleavable cationic gemini surfactant: a potential system for solubilization and release of ibuprofen. J. Mol. Liq. 366, 120311.
Lee, S.-Y., Tyler, J.Y., Kim, S., Park, K., Cheng, J.-X., 2013. FRET imaging reveals different cellular entry routes of self-assembled and disulfide bonded polymeric micelles. Mol. Pharm. 10, 3497–3506.
Lee, K., Lee, J., Lee, S.G., Park, S., Yang, D.S., Lee, J.-J., Khademhosseini, A., Kim, J.S., Ryu, W., 2020. Microneedle drug eluting balloon for enhanced drug delivery to vascular tissue. J. Control. Release 321, 174–183.
Lee, S., Yoon, C.-H., Oh, D.H., Anh, T.Q., Jeon, K.-H., Chae, I.-H., Park, K.D., 2023. Gelatin microgel-coated balloon catheter with enhanced delivery of everolimus for long-term vascular patency. Acta Biomater. 173, 314–324.
Lemos, P.A., Farooq, V., Takimura, C.K., Gutierrez, P.S., Virmani, R., Kolodgie, F., Christians, U., Kharlamov, A., Doshi, M., Sojitra, P., van Beusekom, H.M., Serruys, P. W., 2013. Emerging technologies: polymer-free phospholipid encapsulated sirolimus nanocarriers for the controlled release of drug from a stent-plus-balloon or a stand-alone balloon catheter. EuroIntervention 9, 148–156.
Li, G., Qiao, H., Lin, H., Wang, R., Chen, F., Li, S., Yang, W., Yin, L., Cen, X., Zhang, Y., Cheng, X., Wang, A.Y.-C., 2022. Application of drug-coated balloons for intracranial atherosclerosis disease: a systematic review. Clin. Neurol. Neurosurg. 213, 107065.
Libby, P., Buring, J.E., Badimon, L., Hansson, G.K., Deanfield, J., Bittencourt, M.S., Tokgozoglu, L., Lewis, E.F., 2019. Atherosclerosis. Nat. Rev. Dis. Primers 5, 56.
Ma, Y., Guan, R., Gao, S., Song, W., Liu, Y., Yang, Y., Liu, H., 2020. Designing orodispersible films containing everolimus for enhanced compliance and bioavailability. Expert Opin. Drug Deliv. 17, 1499–1508.
Maki, M.A.A., Kumar, P.V., Cheah, S.-C., Siew Wei, Y., Al-Nema, M., Bayazeid, O., Majeed, A.B.B.A., 2019. Molecular modeling-based delivery system enhances everolimus-induced apoptosis in Caco-2 cells. ACS Omega 4, 8767–8777.
Maysinger, D., Lovrić, J., Eisenberg, A., Savić, R., 2007. Fate of micelles and quantum dots in cells. Eur. J. Pharm. Biopharm. 65, 270–281.
Nelemans, L.C., Gurevich, L., 2020. Drug delivery with polymeric nanocarriers-cellular uptake mechanisms. Materials (Basel) 13, 366.
Nguyen, V.T., Nguyen, Q.T., Pham, N.T., Nguyen, D.T., Pham, T.N., Tran, N.Q., 2021. An in vitro investigation into targeted paclitaxel delivery nanomaterials based on chitosan-Pluronic P123-biotin copolymer for inhibiting human breast cancer cells. J. Drug Deliv. Sci. Technol. 66, 102807.
Park, D.S., Bae, I.-H., Jeong, M.H., Lim, K.S., Sim, D.S., Hong, Y.J., Lee, S.-Y., Jang, E.J., Shim, J.-W., Park, J.-K., Lim, H.C., Kim, H.B., 2018. In vitro and in vivo evaluation of a novel polymer-free everolimus-eluting stent by nitrogen-doped titanium dioxide film deposition. Mater. Sci. Eng. C 91, 615–623.
Patel, H.S., Shaikh, S.J., Ray, D., Aswal, V.K., Vaidya, F., Pathak, C., Varade, D., Rahdar, A., Sharma, R.K., 2022. Structural transitions in mixed Phosphatidylcholine/Pluronic micellar systems and their in vitro therapeutic evaluation for poorly water-soluble drug. J. Mol. Liq. 364, 120003.
Sahu, A., Kasoju, N., Goswami, P., Bora, U.J., 2011. Encapsulation of curcumin in Pluronic block copolymer micelles for drug delivery applications, 25, 619–639.
Sastry, N.V., Hoffmann, H., 2004. Interaction of amphiphilic block copolymer micelles with surfactants. Colloids Surf. A Physicochem. Eng. Asp. 250, 247–261.
Song, H., He, R., Wang, K., Ruan, J., Bao, C., Li, N., Ji, J., Cui, D., 2010. Anti-HIF-1α antibody-conjugated pluronic triblock copolymers encapsulated with Paclitaxel for tumor targeting therapy. Biomaterials 31, 2302–2312.
Tang, Z., Yin, L., Zhang, Y., Yu, W., Wang, Q., Zhan, Z., 2019. Preparation and study of two kinds of ophthalmic nano-preparations of everolimus. Drug Deliv. 26, 1235–1242.
Tesfamariam, B., 2016. Local arterial wall drug delivery using balloon catheter system. J. Control. Release 238, 149–156.
Tzafriri, A.R., Parikh, S.A., Edelman, E.R., 2019. Taking paclitaxel coated balloons to a higher level: predicting coating dissolution kinetics, tissue retention and dosing dynamics. J. Control. Release 310, 94–102.
Ulu, A., Aygün, T., Birhanlı, E., Ateş, B., 2022. Preparation, characterization, and evaluation of multi–biofunctional properties of a novel chitosan–carboxymethylcellulose–Pluronic P123 hydrogel membranes loaded with tetracycline hydrochloride. Int. J. Biol. Macromol. 222, 2670–2682.
van den Berg, J.C., 2017. Drug-eluting balloons for treatment of SFA and popliteal disease - a review of current status. Eur. J. Radiol. 91, 106–115.

Wang, Y., Ma, Y., Gao, P., Chen, Y., Yang, B., Feng, Y., Jiao, L., 2020. Paclitaxel coated balloon vs. bare metal stent for endovascular treatment of symptomatic vertebral artery origin stenosis patients: protocol for a randomized controlled trial. Front. Neurol. 11, 579238.

Wang, L., Li, X., Li, T., Liu, L., Wang, H., Wang, C., 2023a. Novel application of drug-coated balloons in coronary heart disease: a narrative review. Front. Cardiovasc. Med. 10, 1055274.

Wang, X., Yang, S., Li, Y., Jin, X., Lu, J., Wu, M., 2023b. Role of emodin in atherosclerosis and other cardiovascular diseases: Pharmacological effects, mechanisms, and potential therapeutic target as a phytochemical. Biomed. Pharmacother. 161, 114539.

Woolford, S.E., Tran, M., NguyenPho, A., McDermott, M.K., Oktem, B., Wickramasekara, S., 2019. Optimization of balloon coating process for paclitaxel coated balloons via micro-pipetting method. Int. J. Pharmaceut. 554, 312–321.

Woolford, S., Tran, M., Yoda, C., Oktem, B., NguyenPho, A., McDermott, M., Wickramasekara, S., 2022. Studying the effect of drug-to-excipient ratio on drug release profile for drug coated balloons. Int. J. Pharmaceut. 620, 121749.

Wyttenbach, N., Kuentz, M., 2017. Glass-forming ability of compounds in marketed amorphous drug products. Eur. J. Pharm. Biopharm. 112, 204–208.

Xiong, G.M., Ang, H., Lin, J., Lui, Y.S., Phua, J.L., Chan, J.N., Venkatraman, S., Foin, N., Huang, Y., 2016. Materials technology in drug eluting balloons: current and future perspectives. J. Control. Release 239, 92–106.

Xue, Q., Yu, T., Wang, Z., Fu, X., Li, X., Zou, L., Li, M., Cho, J.Y., Yang, Y., 2023. Protective effect and mechanism of ginsenoside Rg2 on atherosclerosis. J. Ginseng Res. 47, 237–245.

Yerasi, C., Case, B.C., Forrestal, B.J., Torguson, R., Weintraub, W.S., Garcia-Garcia, H.M., Waksman, R., 2020. Drug-coated balloon for De Novo coronary artery disease: JACC state-of-the-art review. J. Am. Coll. Cardiol. 75, 1061–1073.

Zhang, Z., Ekanem, E.E., Nakajima, M., Bolognesi, G., Vladisavljević, G.T., 2022. Monodispersed sirolimus-loaded PLGA microspheres with a controlled degree of drug–polymer phase separation for drug-coated implantable medical devices and subcutaneous injection. ACS Appl. Bio Mater. 5, 3766–3777.